Applied Physics Letters ARTICLE scitation.org/journal/apl

Ultrahigh photovoltage responsivity of PEDOT:PSS–silicon hybrid heterojunction photodiodes

Cite as: Appl. Phys. Lett. **117**, 073301 (2020); doi: 10.1063/5.0007685
Submitted: 19 March 2020 · Accepted: 7 August 2020 ·
Published Online: 18 August 2020

Amirhossein Mosaddegh, Aliakbar Noroozi, Mohammad Javadi,[a] and Yaser Abdi[b]

AFFILIATIONS

Nanophysics Research Laboratory, Department of Physics, University of Tehran, Tehran 14395-547, Iran

[a]Author to whom correspondence should be addressed: m_javadi_b@ut.ac.ir
[b]Electronic mail: y.abdi@ut.ac.ir

ABSTRACT

Strong inversion at the poly(3,4-ethylenedioxythiophene): polystyrene sulfonate PEDOT:PSS/silicon interface facilitates the separation of excess carriers and obstructs surface recombination, both are of utmost importance for optoelectronic detectors. In this view, low-temperature solution-processed PEDOT:PSS/silicon hybrid heterojunctions possess great potential for light detection applications. We investigate the performance of hybrid PEDOT:PSS/silicon photodetectors following long-period exposure to ambience. In addition, the effect of PEDOT:PSS conductivity on the performance of hybrid heterojunction photodiodes is also explored. In the self-powered photovoltage mode, the hybrid photodiode displays an ultrahigh responsivity of 10^6 V/W, a noise equivalent power of 10 pW/$\sqrt{\text{Hz}}$, and a detectivity up to 10^{10} Jones. Thermal noise is identified as the main limiting factor in the device performance. The hybrid photodetector demonstrates a desirable stability over long-time storage in air.

Emerging materials draw great attention from both fundamental and applied perspectives for their potential to uncover unprecedented physical concepts and improve device performance. However, most of these materials share common challenges in the development toward global commercialization. They are expected to provide compatible benefits in view of performance, price, and stability, particularly in competition with the mature silicon technology. An approach to make use the properties of these materials is hybridizing them into silicon-based devices with the goal of upgrading existing technology in terms of higher performance and reduced production cost. Organic polymers like poly(3,4-ethylenedioxythiophene) polystyrene sulfonate (PEDOT:PSS)[1–9] and two-dimensional materials as graphene[10,11] are the most promising pioneers of such hybridization with wide applications in solar cells and photodiodes. Solution-processed composite conductive polymer PEDOT:PSS with excellent mechanical and thermal stability provides a rapid, low-temperature, vacuum-free, and hence low-cost production of hybrid electronic and optoelectronic devices. Intensive research has been done on hybrid organic–inorganic PEDOT:PSS/Si solar cells where PEDOT:PSS serves as a transparent, hole-extracting electrode.[12] Meanwhile, this hybrid heterojunction displays interesting physical properties, namely, interfacial inversion layer,[13–15] strong band bending beyond the Mott–Schottky limit,[16] and hybrid charge transport mechanism.[17]

In spite of extensive studies on the hybrid PEDOT:PSS/Si solar cells, which led to a record efficiency of 16% (Refs. 18 and 19) in a nearly short period of time [the efficiency limit is theoretically predicted to be around 20% (Ref. 4)], there are only a few studies on other optoelectronic devices based on PEDOT:PSS/Si hybrids. A hybrid device based on PEDOT:PSS and silicon nanowires is demonstrated as a self-powered, broad-band, and high-speed photodetector, which exhibits a response bandwidth of 40 kHz and a fast rise time of 2 μs.[20] A graphene quantum-dot modified PEDOT:PSS/Si hybrid with a noticeable photocurrent responsivity of 1 A/W at 2.5 μW is proven to be an excellent candidate for omnidirectional weak light harvesting.[21,22] A hybrid PEDOT:PSS/Si optical position-sensitive detector with a high sensitivity of 100 mV/mm and an excellent non-linearity of 3% is reported by the authors,[23] and more recently, a solar-blind UV photodetector based on hybrid PEDOT:PSS/Ga_2O_3/Si with UV-visible rejection as high as 450 is reported displaying a quantum efficiency of 15%, a record much higher than that of the conventional Ga_2O_3 ultraviolet photodetectors.[24]

The excellent results of the above studies indicate the great potential of hybrid PEDOT:PSS/Si for light detection. In this regard, hybrid organic–inorganic photodetectors (HOIPs) deserve to be the subject of much more studies. Nonetheless, a collective standard characterization of the planar PEDOT:PSS/Si has not been carried out yet and the prime capabilities of such hybrid detectors are vague. Previous studies provide the performance of hybrid photodetectors in the high (mW) and moderate (μW) optical powers, and the photoresponse of HOIPs upon extreme low intensities is unclear. In addition, the effect of background noise as the ultimate limiting factor in the photodetector performance was not considered properly, which may lead to underestimated noise equivalent power (NEP) and inflated specific detectivity.[25] Moreover, during long-term storage of PEDOT:PSS/Si in ambience, humidity-related polymer deterioration (due to the hygroscopic nature of the PSS group)[18,26,27] and interfacial suboxide augmentation[27] lead to S-shaped J–V curves and severe reduction of the fill-factor and open-circuit. Hence, it is indispensable to investigate the performance of HOIPs following long-term storage in air.

Herein, we investigate the photodetection properties of PEDOT:PSS/Si planar heterojunction photodiodes in the self-powered photovoltage mode. The performance of HOIPs in a broad range of optical powers from nW to mW is studied, and the characteristic figures of merit are extracted utilizing standardized techniques. We have also studied the effect of PEDOT:PSS conductivity on the optical signal detection. In order to explore the stability of HOIPs, we carried out the experiments after long-term storage of the fabricated HOIPs in ambience.

The electrical conductivity of PEDOT:PSS considerably improves through the addition of polar organic solvents like dimethyl sulfoxide (DMSO) and ethylene glycol into PEDOT:PSS aqueous solution.[28,29] We carried out organic solvent treatment by adding DMSO solution into aqueous PEDOT:PSS (Ossila, PH1000). The four-point conductivity of pristine and 5% DMSO-treated PEDOT:PSS thin films is determined as 0.26 and 792 S cm^{-1} in accord with earlier reports.[28,30] DMSO can be considered as the PSS solvent where the thickness of the insulator PSS shell around conductive PEDOT grains reduces through DMSO-treatment.[31] Lightly n-doped silicon (1–10 Ω cm) with 300 nm SiO_2 is used to fabricate hybrid photodetectors. We have utilized dilute buffered HF solution to etch the SiO_2 layer on selected regions. In order to prevent surface oxidation, silicon samples were dried and kept under a nitrogen atmosphere prior to the deposition of organic layer. To increase the wettability of PEDOT:PSS, Triton X-100 solvent (1%w) was also added to the aqueous solutions. PEDOT:PSS was spin-coated onto the silicon surface at 2000 rpm for 60 s. The samples were then heated at 110 °C for 30 min under N_2 stream.[32] A 150-nm-thick Au film was thermally evaporated onto an organic layer using a shadow mask. Low-temperature Ohmic contacts to n-Si were obtained by thermal evaporation of Au/Sb (0.98/0.2%w) onto the back side of silicon.[33] The scanning electron micrograph and a cross-sectional scheme of the fabricated HOIPs are shown in Fig. 1. The active area of the pristine and DMSO-treated HOIPs is A = 4 and A = 6.25 mm^2, respectively. To ensure performance stabilization, the fabricated HOIPs were kept in the ambience for 20 days prior to performing experiments (supplementary material S1).

Current–voltage characteristics of the DMSO-treated HOIP under different intensities of 656 nm illumination are shown in Fig. 1(c). Although the energy of incident photons (1.9 eV) is higher than

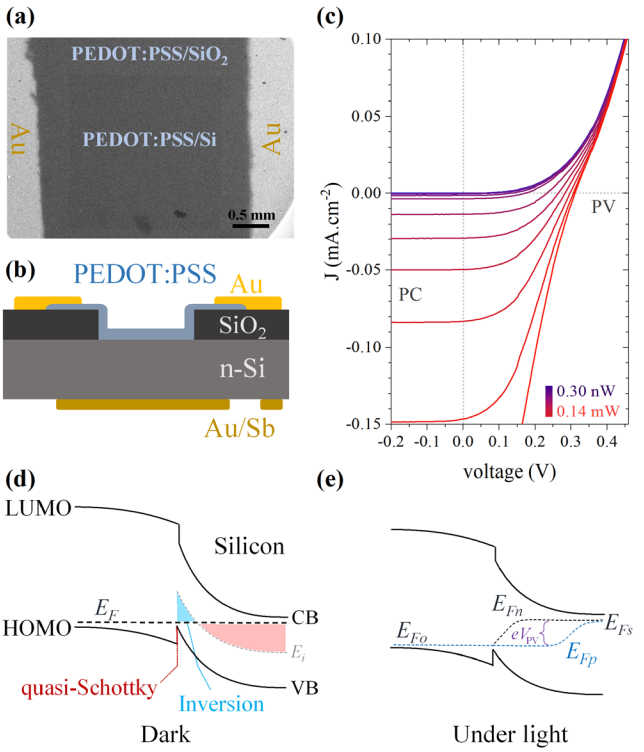

FIG. 1. (a) Scanning electron micrograph and (b) a cross section scheme of the PEDOT:PSS/Si HOIP. (c) Steady-state current–voltage characteristic of the DMSO-treated HOIP under different intensities of 656 nm illumination. (d) and (e) Energy band alignment at the hybrid interface in equilibrium and upon illumination (open-circuit).

the bandgap of both PEDOT:PSS ($E_{gap} \cong 1.6$ eV) and silicon ($E_{gap} = 1.12$ eV), owing to the relative thinness of PEDOT:PSS (~100 nm), the organic layer is almost transparent (>90%, supplementary material S2), and, hence, to a good degree, all the incident photons are absorbed by silicon. In addition, since the skin depth of 655 nm photons into silicon is around 5 μm, a substantial portion of incident photons is absorbed in bulk, i.e., far from the depletion region at the interface. The quasi-Fermi level of PEDOT:PSS lies in the vicinity of the highest occupied molecular orbital (HOMO), representative of a p-type semiconductor. Hence, as depicted in Fig. 1(d), the junction at the p-PEDOT:PSS/n-Si interface is a type-II staggered Pn heterojunction where the mismatch of bandgaps leads to the formation of a quasi-Schottky barrier for hole injection from n-Si into p-PEDOT:PSS.[17] In addition, due to the relatively high work function of PEDOT:PSS (4.7–5.2 eV), an inversion layer is developed at the interface.[13–16] The thickness of the inversion layer is typically less than 2 nm and reduces with the strength of the internal electric field at the interface.[34] Surface recombination of excess photogenerated carriers has a profound effect on the photoresponse of photodiodes. Upon inversion, the density of excess electrons at the surface of n-type silicon reduces considerably, leading to a slow surface recombination velocity. Indeed, the presence of the inversion layer induces an internal p–n junction where the minority holes in the bulk of n-Si become majority carriers at the surface [Fig. 1(d)]. In this regard, the separation of

excess photogenerated carriers is accomplished within silicon itself and the recombination velocity at the surface of n-Si is suppressed.[13] This explains the appreciable photoresponse of PEDOT:PSS/Si HOIPs.

Upon illumination and under open-circuit conditions, a photovoltage $V_{PV} = V_{light} - V_{dark}$ is developed across the junction [Fig. 1(e)]. Photovoltage vs optical power is presented in Fig. 2(a). From the lowest measured intensity (0.3 nW) to the onset of saturation at 6.2 μW, photovoltage remains as a constant-power function of incident light intensity ($V_{PV} = \alpha P^{\beta}$), indicating a proper response over more than four decades of incident intensity. The photovoltage responsivity ($R_V = V_{PV}/P$) of HOIPs is shown in Fig. 2(b) where the responsivity of DMSO-treated PEDOT:PSS/Si exceeds 2×10^6 V/W at lower intensities. This record is comparable with the recently developed ultrasensitive graphene/silicon Schottky photodetectors.[35] We noted that R_V exhibits two distinct power-law dependences on the incident light intensity, which are fairly separated at 6.2 μW. At higher optical powers, responsivity is proportional to the inverse of incident power $R_V \propto P^{-1}$, while for $P \leq 6.2$ μW, the responsivity is well characterized by $R_V \propto P^{-0.4}$. Since photovoltage is directly related to the splitting of electron and hole quasi-Fermi levels by $eV_{PV} = E_{Fn} - E_{Fp}$ [see Fig. 1(e)], the responsivity should strongly depend on the majority carrier concentration as well as total density of states at the band edges. Indeed, the open-circuit voltage of hybrid PEDOT:PSS/Si solar cells is very sensitive to the dopant density in silicon,[14,36] corroborating the aforementioned relationship. In this regard, the functional dependence of responsivity on the optical power somehow reflects the total density of states, and the appearance of the sub-linear regime may originate from the presence of band tails with a finite density (e.g., dopant levels) governing photovoltage response at the low intensities of incident light.

The noise equivalent power (NEP) of the HOIPs is directly determined by performing fast-Fourier transform on voltage vs time data. To measure NEP, the modulation frequency of incident light and the oscilloscope integration time were set to 14 Hz and 4 ms, respectively. The spectral voltage density of the DMSO-treated sample at different incident powers is shown in Fig. 2(c) where the rms dark noise density is obtained as $S_V \cong 3.1 \times 10^{-7}$ V/$\sqrt{\text{Hz}}$. Both HOIPs exhibit white noise character with no signature of Flicker $1/f$-noise down to 1 Hz. Johnson–Nyquist thermal noise density per unit of bandwidth is given by $V_{th} = \sqrt{4k_B TR}$, where R stands for device resistance. Utilizing differential dark resistance of the DMSO-treated HOIP (R = 18.4 kΩ at V = 0.3 V), we obtain $V_{th} = 1.8 \times 10^{-8}$ V/$\sqrt{\text{Hz}}$. For the pristine sample with the measured $S_V \cong 3.7 \times 10^{-7}$ V/$\sqrt{\text{Hz}}$ and R = 189.4 kΩ at V = 0.3 V, the thermal noise is estimated to be $V_{th} = 5.6 \times 10^{-8}$ V/$\sqrt{\text{Hz}}$. Utilizing zero-bias differential resistance, the measured dark noise becomes even more consistent with the theoretical thermal noise (see supplementary material S4). Since the measured dark noise density of HOIPs fairly coincides with the Johnson–Nyquist white noise, we conclude that the ultimate photovoltage sensitivity of HOIPs upon low-level intensities is limited by the background thermal noise.

The signal-to-noise ratio (SNR) of the HOIPs, extracted from spectral photovoltage density, is shown in Fig. 2(d). At the lowest tested intensity, we obtained a SNR of 5.9 and 11.5 for the pristine and DMSO-treated HOIPs, respectively. The improved SNR of the latter originates from the enhanced conductivity of the organic layer, which leads to a lower thermal noise as discussed above. Since NEP is the power of incident light at which SNR = 1, we infer that the actual NEP of both HOIPs is lower than 10^{-9} W/$\sqrt{\text{Hz}}$. Linear extrapolation of the SNR steers toward NEP = 23 pW/$\sqrt{\text{Hz}}$ and NEP = 14 pW/$\sqrt{\text{Hz}}$ for pristine and DMSO-treated HOIPs, respectively. The specific detectivity can be directly calculated from $D^* = \sqrt{A}/\text{NEP}$. Utilizing this equation, we obtain a minimum detectivity of $D^* = 2 \times 10^8$ Jones for both HOIPs (Jones = cm $\sqrt{\text{Hz}}$/W). Considering linear extrapolation, the DMSO-treated PEDOT:PSS/Si conducts to an appreciable detectivity of $D^* = 1.8 \times 10^{10}$ Jones in the self-powered photovoltage mode.

Dynamical characteristics of HOIPs are presented in Fig. 3. Figure 3(a) shows normalized photovoltage as a function of modulation frequency of the incident light. The response bandwidths can be inferred from the −3 dB line, which for pristine and DMSO-treated HOIPs are obtained as B = 37 Hz and B = 450 Hz, respectively. In order to find out the origin of this difference, we have investigated the photovoltage response and recovery vs time [Figs. 3(b) and 3(c)]. The DMSO-treated HOIP exhibits a characteristic 10%–90% rise time of 47 μs, which is almost six times faster than the pristine HOIP. We attribute this faster rise time to the enhanced conductivity of the DMSO-treated organic layer. Similarly, the decay time of the DMSO-treated HOIP is around 11 ms much smaller than that of the pristine HOIP with a recovery time of 330 ms. Since the photovoltage rise times of HOIPs are much smaller the corresponding fall times, we conclude that it is the photovoltage decay that ultimately places a limit on the response bandwidth. The decay of the photovoltage response is

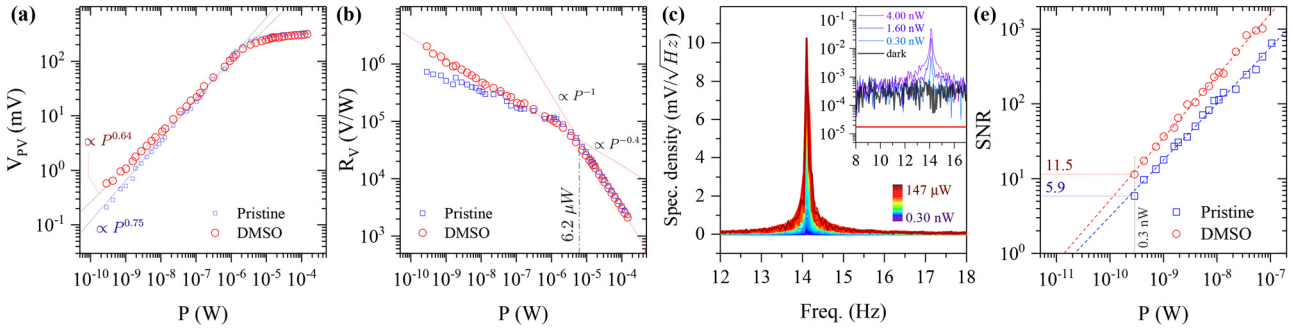

FIG. 2. (a) Photovoltage vs intensity of incident light. Dashed lines represent power-law fittings to the experimental data. (b) Responsivity as a function of illumination power. (c) Photovoltage spectral density of the DMSO-treated PEDOT:PSS/Si measured at a light modulation frequency of 14 Hz. The inset represents the spectral density at low incident powers. The red line shows the Johnson–Nyquist thermal noise limit. (e) SNR of HOIPs. The dashed lines are linear extrapolation to SNR = 1.

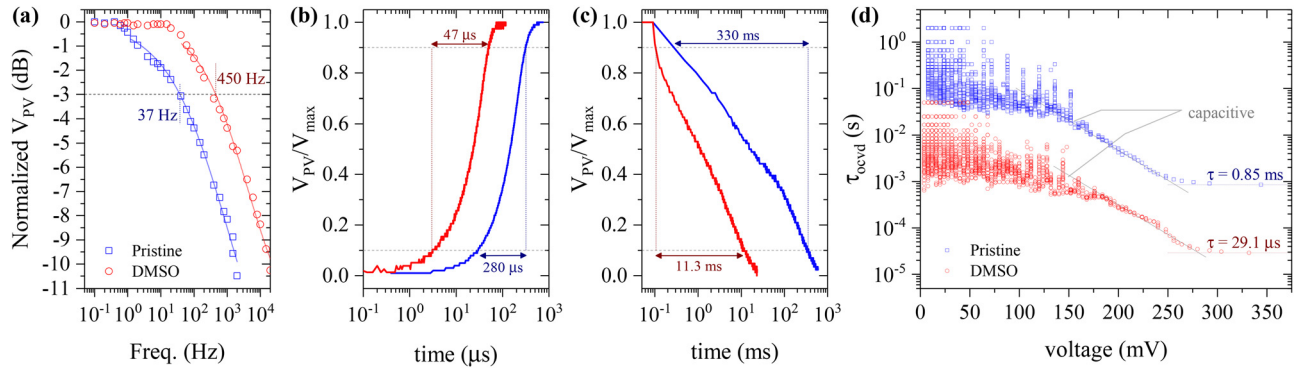

FIG. 3. (a) Normalized photovoltage ($10\log[V_{PV}(f)/V_{PV}(0.1\,\text{Hz})]$) vs modulation frequency of incident light. (b) and (c) Photovoltage response and recovery processes. Blue and red lines represent dynamics of pristine and DMSO-treated PEDOT:PSS/Si, respectively. (d) Lifetime of excess photogenerated carriers extracted from OCVD. Lines are guides to eye.

mainly governed by two effects, namely, the lifetime of excess carriers and the time required for the discharge of interface capacitance.[37] In this regard, the limited bandwidth of HOIPs implies a (small) persistent photovoltage, which may originate from either prolonged lifetime of excess carriers or slow discharge of interface depletion capacitance.

We have employed the open-circuit voltage decay (OCVD) technique to find out whether these factors restrict the recovery time of the photodetectors. In this approach, τ_{ocvd} is related to the lifetime of carriers (τ) and the discharge time of interface capacitance (τ_{cap}) through $\tau_{ocvd} = -\frac{k_B T}{e}\left(\frac{dV_{OC}}{dt}\right)^{-1} = \tau + \tau_{cap}$, where τ and τ_{cap} dominate the voltage decay data at the high and low voltages, respectively.[37] From the high voltage region in Fig. 3(d), the lifetime of excess carriers in pristine and DMSO-treated HOIPs is determined as 0.85 ms and 29.1 μs. While the pristine sample shows a prolonged lifetime, the lifetime of minority carriers in the DMSO-treated PEDOT:PSS/Si is in good agreement with the previous studies.[15,38,39] At the lower voltages, the capacitive term of pristine and DMSO-treated HOIPs tends to 10^{-1} and 10^{-2} s. This clarifies that the slow discharge of depletion capacitance is the main origin for the limited response bandwidth. The photovoltage decay time observed here is much higher than that in the previous report,[20] more probably due to the long-time exposure of HOIPs to ambience where the interfacial suboxide augments in terms of thickness and degree of oxidation.[27]

Finally, as represented in supplementary material S5, the HOIPs exhibit steady output over cyclic continuous operation with no sign of drift. Also, following long-term exposure to ambience and within a period of ten days, the photovoltage response drops by less than 2%, demonstrating a desirable stability for regular applications.

In summary, the performance of PEDOT:PSS/Si hybrid photodetectors in the self-powered photovoltage mode is investigated after long-term storage of the detectors in ambience. We show that in a simple planar geometry, PEDOT:PSS/Si HOIPs exhibit an ultrahigh photovoltage responsivity of 10^6 V/W with a specific detectivity of 10^{10} Jones, which indicates the reliable capability of these hybrid heterojunctions for the optical signal detection. Owing to the higher conductivity of DMSO-treated PEDOT:PSS, the corresponding HOIP exposes improved responsivity, SNR, detectivity, and response bandwidth when compared with the pristine PEDOT:PSS/Si.

See the supplementary material for the properties of the organic layer, current–voltage characteristics, spectral density, and stability.

AUTHORS' CONTRIBUTIONS

A.M. and A.N. contributed equally to this work.

The authors acknowledge "Iran's National Elites Foundation (INEF)" and "Iran Science Elites Federation (ISEF)" for partial financial support.

DATA AVAILABILITY

The data that support the findings of this study are available within this article and its supplementary material.

REFERENCES

[1]E. L. Williams, G. E. Jabbour, Q. Wang, S. E. Shaheen, D. S. Ginley, and E. A. Schiff, Appl. Phys. Lett. **87**, 223504 (2005).
[2]S.-C. Shiu, J.-J. Chao, S.-C. Hung, C.-L. Yeh, and C.-F. Lin, Chem. Mater. **22**, 3108 (2010).
[3]B. Ozdemir, M. Kulakci, R. Turan, and H. E. Unalan, Appl. Phys. Lett. **99**, 113510 (2011).
[4]T.-G. Chen, B.-Y. Huang, E.-C. Chen, P. Yu, and H.-F. Meng, Appl. Phys. Lett. **101**, 033301 (2012).
[5]S. Jeong, E. C. Garnett, S. Wang, Z. Yu, S. Fan, M. L. Brongersma, M. D. McGehee, and Y. Cui, Nano Lett. **12**, 2971 (2012).
[6]M. Wang, H. Wang, W. Li, X. Hu, K. Sun, and Z. Zang, J. Mater. Chem. A **7**, 26421 (2019).
[7]X. Zeng, T. Zhou, C. Leng, Z. Zang, M. Wang, W. Hu, X. Tang, S. Lu, L. Fang, and M. Zhou, J. Mater. Chem. A **5**, 17499 (2017).
[8]M. Wang, Z. Zang, B. Yang, X. Hu, K. Sun, and L. Sun, Sol. Energy Mater. Sol. Cells **185**, 117 (2018).
[9]X. Liu, M. Wang, F. Wang, T. Xu, Y. Li, X. Peng, H. Wei, Z. Guan, and Z. Zang, IEEE Electron Device Lett. **41**, 1044 (2020).
[10]A. D. Bartolomeo, Phys. Rep. **606**, 1 (2016).
[11]S. K. Behura, C. Wang, Y. Wen, and V. Berry, Nat. Photonics **13**, 312 (2019).
[12]P. Gao, Z. Yang, J. He, J. Yu, P. Liu, J. Zhu, Z. Ge, and J. Ye, Adv. Sci. **5**, 1700547 (2018).
[13]A. S. Erickson, A. Zohar, and D. Cahen, Adv. Energy Mater. **4**, 1301724 (2014).
[14]S. Jäckle, M. Mattiza, M. Liebhaber, G. Brönstrup, M. Rommel, K. Lips, and S. Christiansen, Sci. Rep. **5**, 13008 (2015).
[15]J. Zhu, X. Yang, J. Sheng, P. Gao, and J. Ye, ACS Appl. Energy Mater. **1**, 2874 (2018).

[16]R. Wang, Y. Wang, C. Wu, T. Zhai, J. Yang, B. Sun, S. Duhm, and N. Koch, Adv. Funct. Mater. **30**, 1903440 (2020).
[17]M. Javadi, A. Mazaheri, H. Torbatiyan, and Y. Abdi, Phys. Rev. Appl. **12**, 034002 (2019).
[18]J. He, P. Gao, Z. Yang, J. Yu, W. Yu, Y. Zhang, J. Sheng, J. Ye, J. C. Amine, and Y. Cui, Adv. Mater. **29**, 1606321 (2017).
[19]H.-D. Um, D. Choi, A. Choi, J. H. Seo, and K. Seo, ACS Nano **11**, 6218 (2017).
[20]Z. Liang, P. Zeng, P. Liu, C. Zhao, W. Xie, and W. Mai, ACS Appl. Mater. Interfaces **8**, 19158 (2016).
[21]M.-L. Tsai, W.-R. Wei, L. Tang, H.-C. Chang, S.-H. Tai, P.-K. Yang, S. P. Lau, L.-J. Chen, and J.-H. He, ACS Nano **10**, 815 (2016).
[22]M.-L. Tsai, D.-S. Tsai, L. Tang, L.-J. Chen, S. P. Lau, and J.-H. He, ACS Nano **11**, 4564 (2017).
[23]M. Javadi, M. Gholami, H. Torbatiyan, and Y. Abdi, Appl. Phys. Lett. **112**, 113302 (2018).
[24]D. Zhang, W. Zheng, R. Lin, Y. Li, and F. Huang, Adv. Funct. Mater. **29**, 1900935 (2019).
[25]Y. Fang, A. Armin, P. Meredith, and J. Huang, Nat. Photonics **13**, 1 (2019).
[26]J. Schmidt, V. Titova, and D. Zielke, Appl. Phys. Lett. **103**, 183901 (2013).
[27]S. Jäckle, M. Liebhaber, J. Niederhausen, M. Büchele, R. Félix, R. G. Wilks, M. Bär, K. Lips, and S. Christiansen, ACS Appl. Mater. Interfaces **8**, 8841 (2016).
[28]H. Shi, C. Liu, Q. Jiang, and J. Xu, Adv. Electron. Mater. **1**, 1500017 (2015).
[29]Q. Wei, M. Mukaida, Y. Naitoh, and T. Ishida, Adv. Mater. **25**, 2831 (2013).
[30]J.-S. Yeo, J.-M. Yun, D.-Y. Kim, S. Park, S.-S. Kim, M.-H. Yoon, T.-W. Kim, and S.-I. Na, ACS Appl. Mater. Interfaces **4**, 2551 (2012).
[31]M. Pietsch, M. Y. Bashouti, and S. Christiansen, J. Phys. Chem. C **117**, 9049 (2013).
[32]X. Shen, Y. Zhu, T. Song, S.-T. Lee, and B. Sun, Appl. Phys. Lett. **103**, 013504 (2013).
[33]J. H. Werner, U. Spadaccini, and F. Banhart, J. Appl. Phys. **75**, 994 (1994).
[34]G. Baccarani and M. R. Wordeman, IEEE Trans. Electron Devices **30**, 1295 (1983).
[35]X. An, F. Liu, Y. J. Jung, and S. Kar, Nano Lett. **13**, 909 (2013).
[36]M. J. Price, J. M. Foley, R. A. May, and S. Maldonado, Appl. Phys. Lett. **97**, 083503 (2010).
[37]D. Kiermasch, A. Baumann, M. Fischer, V. Dyakonov, and K. Tvingstedt, Energy Environ. Sci. **11**, 629 (2018).
[38]Y. Zhang, W. Cui, Y. Zhu, F. Zu, L. Liao, S.-T. Lee, and B. Sun, Energy Environ. Sci. **8**, 297 (2015).
[39]J. Zhu, X. Yang, Z. Yang, D. Wang, P. Gao, and J. Ye, Adv. Funct. Mater. **28**, 1705425 (2018).